Downwind Sound Propagation in an Atmospheric Boundary Layer

William E. Zorumski* and William L. Willshire Jr.†
NASA Langley Research Center, Hampton, Virginia

A theoretical analysis is given for an acoustic monopole in an atmospheric boundary layer. The analysis is based on the Obukhov quasipotential function (which defines both acoustic pressure and velocity) and assumes an isothermal atmosphere, an exponential boundary-layer flow profile, and a ground impedance function. It is shown that acoustic waves in the boundary layer can be represented by plane waves with variable amplitude. The wave amplitudes are given by the generalized hypergeometric function ${}_0F_1$. The present work is an extension of previous work by Wenzel, who studied surface waves associated with a ground plane without flow, and by Chunchuzov, who identified a discrete mode spectrum in an exponential boundary layer over a hard surface. It is shown that downwind propagation of low-frequency sound can be represented by these discrete modes, which spread as cylindrical waves. The downwind attenuation of the fundamental mode is proportional to frequency squared, wind speed, boundary-layer displacement thickness, and the real part of the ground admittance. The analysis is supported by acoustic data from a wind turbine at Medicine Bow, Wyoming.

Nomenclature

A = upward-traveling wave amplitude
$(a)_n$ = factorial function, $a(a+1)\cdots(a+n-1)$
b = channel width parameter
B = downward-traveling wave amplitude
c = speed of sound
f = frequency
F = upward-traveling wave, $Ae^{+ik_z z}$
${}_0F_1$ = generalized hypergeometric function
G = downward-traveling wave, $Be^{-ik_z z}$
J_ν = Bessel function of the first kind
k = plane wave number ω/c
k_x, k_y, k_z = wave numbers in x, y, and z directions
L = boundary condition operator
M = Mach number
$\tilde{p}$ = acoustic pressure
p_ν = first Bessel function cross product
q_ν = second Bessel function cross product
Q = volumetric source strength
r, θ, z = cylindrical coordinates
R = spherical radius
SPL = sound pressure level
t = time
$\tilde{u}, \tilde{v}, \tilde{w}$ = acoustic velocities in x, y, and z directions, respectively
U = wind velocity
$W[F,G]$ = Wronskian of F and G
x, y, z = rectangular coordinates, downwind, crosswind, and vertical, respectively
Y_ν = Bessel function of the second kind
α = plane wave attenuation coefficient or downwind attenuation
β = specific ground admittance
$\Gamma(z)$ = complex gamma function
δ_1 = boundary-layer displacement thickness
ϵ = strip width parameter
ζ = waveguide coordinate
Θ = standing wave function
ν = Wronskian
ρ = density
ξ = strip coordinate
Ψ = Obukhov quasipotential
ω = circular frequency
Ω_y = boundary-layer vorticity

Subscripts

m = mode index
n = harmonic number
s = source position
x, r = in the respective coordinate direction
0 = on the ground, $z = 0$
∞ = above the boundary layer, $z \to \infty$

Presented as Paper 86-1923 at the AIAA 10th Aeroacoustics Conference, Seattle, WA, July 9-11, 1986; received Aug. 6, 1986; revision received April 26, 1988.

*Chief Scientist, Acoustics Division. Member AIAA.
†Aerospace Engineer, Acoustics Division.

Introduction

THIS paper will analyze the acoustic field of a source in an atmospheric boundary layer and compare the analysis to the downwind propagation of noise from a wind turbine. The dependent acoustic variable used is the Obukhov quasipotential function,[1] an extension of the conventional acoustic potential[2] which accounts for the effect of steady flow vorticity in the acoustic momentum equation. The analytical model is that of an acoustic monopole above a ground plane with a finite acoustic impedance.[2] The wind boundary layer is modeled by an exponential function to facilitate the analysis.

Wenzel[3] showed that a monopole source over an impedance plane can lead to a surface wave, or inhomogeneous wave, whose amplitude decays exponentially with height above the ground. The mathematical origin of the surface wave is a pole in the plane of complex radial wave number which contributes to the inversion integral if the ground impedance is of the compliant type. Chien and Soroka[4] have expanded on Wenzel's analysis and clarified some points relating to earlier studies of this model. Thomasson[5] showed that Wenzel's exact solution could be given as a computationally efficient integral

along a steepest descent contour plus a Hankel function term. More recently, Nobile and Hayek[6] used an integral identity to remove the troublesome singularity in the transform solution and have developed a very accurate asymptotic computation method valid down to less than a wavelength from the source.

A ground impedance must be defined in order to apply the preceding analyses. Delany and Bazley[7] developed an empirical impedance model for fibrous materials which is a function of a single flow resistance parameter.[1] Chessell[8] showed that the Delany-Bazley formula was a useful model for ground impedance by correlating predictions based on this formula with the overground propagation data of Parkin and Scholes.[9,10] Propagation experiments[11] have been used to measure the ground impedance and to infer the flow resistance parameter in the ground model. Zuckerwar[12] has developed an instrument for the direct measurement of ground impedance. The Delany-Bazley formula has proved to be surprisingly robust, giving useful results for frequencies well below those for which it was intended; however, it appears to fail at the low frequencies to be considered here. Attenborough[13] has developed a multiparameter impedance model that better represents this low-frequency regime. Upon specification of parameters representing the structure of the media, the Attenborough model reduces to a single-parameter (flow resistance) formula at low frequencies. The Attenborough model also defines the properties of the media, not just the surface impedance, and has been used in the analysis of an acoustic monopole over a porous half-space.[14]

The effect of weak temperature gradients on acoustic waves is represented by allowing the sound speed to be variable but dropping terms involving explicit derivatives of the sound speed. Pekeris[15] used this high-frequency approximation to analyze several sound speed profiles that lead to known special functions, principally the linear sound speed profile, leading to a solution expressible in terms of Bessel functions. Brekhovskikh[16] shows that propagation through an Epstein layer, where the sound speed profile is defined by hyperbolic functions, leads to solutions in terms of the hypergeometric function ${}_2F_1$. Van Moorhem and Landheim[17] have developed an approximate solution for a boundary-layer type of thermal profile that has a slow asymptotic approach to a constant value high above the ground. More general thermal profiles may be analyzed with the "fast-field" numerical method of Raspet et al.[18] This method appears to be effective for both temperature lapse and temperature inversion conditions and readily incorporates the ground impedance.

Corrections are available for the effects of atmospheric pressure gradients,[19] but these are important only at frequencies typical of atmospheric buoyancy waves[19] or for large vertical propagation distances. Buoyancy wave frequencies are about two orders of magnitude smaller than those of interest here, and we are considering effects close to the ground, so that pressure gradient effects will be omitted here.

Pridmore-Brown[20] developed general equations, without the weak gradient assumption, for sound propagation including wind, temperature, and pressure gradient effects. He then utilized the Langer approximation to find an estimate for propagation in the upwind shadow zone. More recently, Rasmussen[21] has developed an approximate prediction method for the effects of both wind and temperature using the Rayleigh integral. Rasmussen validated his method with experimental data, both upwind and downwind of the source. His approximations, based on ray-acoustic theory, gave generally good agreement with data at the shorter propagation distances. This agreement deteriorated somewhat at the longer ranges and higher frequencies.

There are few analytic results for acoustic waves in sheared flow. Koutsoyannis[22] has shown that acoustic waves in linearly sheared flow (constant vorticity) may be represented by the Whittaker functions. The Koutsoyannis result is not limited to small Mach number flow but does not include thermal and pressure gradients. Another shear flow where analytic results are possible is the exponential-profile boundary layer. In this case, where the approximation of small Mach number is required, Chunchuzov[23] has shown that the Obukhov quasipotential[2] solution may be represented by Bessel functions of complex order and argument.

Chunchuzov[23] has given the solution for a point source in an exponential boundary layer over a hard surface. His solution is a field that radiates upward like the fields of Wenzel[3] and Thomasson.[5] The presence of the boundary layer causes the downwind field to contain a discrete set of trapped waves or normal modes.[16,23] These normal modes propagate downwind as cylindrical waves, decaying with $1/\sqrt{r}$, the square root of distance. The other term in the downwind field is the lateral wave, which has a spherical spreading character, decaying with $1/r$, the inverse of distance. At long ranges downwind, the normal mode field dominates.

Wind turbine noise measurements by Willshire[24] show the cylindrical-spreading characteristic of a normal mode field. The measurements were made at a wind turbine at Medicine Bow, Wyoming. The turbine is two-bladed, 40 m in diameter, with a hub 80 m above the ground. It rotates at constant speed, producing a fundamental frequency of 1 Hz, presumably due to the cutting of the tower wake by the blades. A ground level microphone array measured frequencies of 5–20 Hz at positions 0.35–20 km downwind. Wind speeds were 25–35 knots, and the boundary-layer profiles could be roughly grouped as thin (about 1 m displacement thickness) during the day and thick (about 50 m displacement thickness) during the night. The effective location of the noise source is near the downward-pointing blade tip, or 40–50 m above the ground. This effective source is therefore above the boundary layer during the day and in the boundary layer at night. Some impedance measurements were made at two sites near the wind turbine using the Zuckerwar meter[12] to check the "typical" quality of the ground.

The cylindrical wave characteristic of Chunchuzov's[23] normal mode analysis coincides with Willshire's observation of a square-root decay law for downwind propagation. This result suggests that the wind turbine's acoustic field may be predictable if the Chunchuzov analysis can be extended slightly to include the position of the source above the ground and the effect of the ground impedance. To this end, our purposes here will be to integrate the analyses of Wenzel[3] and Chunchuzov[23] and to see if the generalized result is consistent with data from the Medicine Bow wind turbine.[25,26]

Acoustic Equations

Propagation Model

The analysis will be based on the model shown in Fig. 1. Rectangular coordinates are defined with x downwind. The xy plane is the ground plane, and an acoustic monopole source S is placed at height z_s above the origin. The acoustic receiver R is at position (x,y,z), with $0 \le z$. The wind has a single component $U(z)$ in the x direction. The wind velocity function $U(z)$ is asymptotic to U_∞ for large z. The analysis is facilitated by assuming a wind velocity profile

$$U(z) = U_\infty(1 - e^{-z/\delta_1}) \tag{1}$$

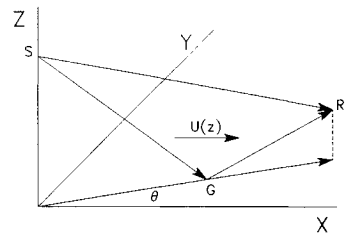

Fig. 1 Geometry for acoustic monopole radiation in an atmospheric wind boundary layer.

and by assuming that the ambient density and sound speed are constants.

The simplistic view of this model is that sound can reach the observer by traveling along the direct ray path SR or along the reflected path SGR. This idea is formalized in the absence of flow and ground surface admittance by constructing the received field as the sum due to the actual source at z_s and an identical "image" source at $-z_s$. When the surface has finite admittance, an additional term, called the "radiated wave" by Wenzel,[3] must be added to the solution for a hard surface. When there is a shear flow present, it is no longer apparent how to construct the field as a superposition of source, image, and radiated waves. It will be seen, however, that the solution of the governing equation and boundary conditions contains these terms in the limit of small wind speeds.

The following analysis is based on Fourier transforms, and in this regard we follow the conventions of Pierce[2] and Brekhovskikh[16] so that the solution in real space is interpreted as the superposition of elementary plane waves of the form $e^{i(k_x x + k_y y - \omega t)}$.

Quasipotential Equations

The acoustic pressure and velocity are given in terms of the Obukhov quasipotential by

$$\tilde{p} = \rho_\infty \frac{d\Psi}{dt} \tag{2}$$

and

$$v = -\nabla \Psi + \int \Omega \times \nabla \Psi \, \partial t \tag{3}$$

The integral in Eq. (3) is at a fixed point in space so that the differential symbol ∂t is used in place of the more conventional symbol dt. The vorticity Ω in our model problem has a single component $U'(z) = U_\infty e^{-z/\delta_1}$ along the y axis. Assuming a monopole of volumetric strength Q the continuity equation is[2,16]

$$\frac{d\tilde{p}}{dt} + \rho_\infty c_\infty^2 \nabla \cdot v = \rho_\infty c_\infty^2 Q \delta(r - r_s) \tag{4}$$

Blokhintsev[1] shows that Eqs. (2) and (3) approximately satisfy the momentum equation provided that $|\Omega|/\omega \ll 1$ and $M \ll 1$. A wave equation for the quasipotential may be formed from Eqs. (2-4) which is valid to the first order in Mach number:

$$\nabla^2 \Psi - \int \nabla \cdot (\Omega \times \nabla \Psi) \, \partial t - \frac{1}{c_\infty^2} \frac{d^2\Psi}{dt^2} = -Q\delta(r - r_s) \tag{5}$$

The Fourier transform of this wave equation converts the total derivative operator $(1/c_\infty)(d/dt)$ into the algebraic factor $-i(k - Mk_x)$. Chunchuzov[23] utilizes the first-order approximation to the square of this factor,

$$(k - Mk_x)^2 \sim (k - M_\infty k_x)^2 + 2kM_\infty k_x e^{-z/\delta_1}, \quad M_\infty \to 0 \tag{6}$$

where the exponential term arises from the assumed wind profile. Another exponential in the wave equation, Eq. (5), is contributed by the vorticity; this term is proportional to k^{-1} due to the time integral. The transform, in time and horizontal spatial dimensions, of the wave equation is thus

$$\frac{d^2\hat{\Psi}}{dz^2} + \left[k_z^2 + aM_\infty \left(\frac{k_x}{\delta_1} \right) e^{-z/\delta_1} \right] \hat{\Psi} = -\frac{\hat{Q}}{4\pi^2} \delta(z - z_s) \tag{7}$$

where

$$a = 2k\delta_1 + 1/(k\delta_1) \tag{8}$$

and k_z is the vertical wave number defined by the dispersion relation[1] for the waves in the uniform flow at infinity. If we let

$$k_r e^{i\phi} = (k_x + M_\infty k) + ik_y \tag{9}$$

then

$$k_z = \sqrt{k^2 - k_r^2}, \qquad \mathrm{Im}(k_z) > 0 \tag{10}$$

In defining k_z, we imagine that k has a small imaginary part α that represents the attenuation rate of a plane wave. Branch cuts, $\mathrm{Im}(k_z) = 0$, in the k_r plane are then segments of hyperbolae extending from the branch points, $k_r = \pm(k + i\alpha)$, to approach the imaginary axes at $\pm i\infty$.

$$L = -\frac{d}{dz} + \frac{M_\infty \cos\phi}{k\delta_1} k_r - i\beta k \tag{11}$$

The ground plane boundary condition is then compactly expressed as

$$L\hat{\Psi}(0) = 0 \tag{12}$$

Solution in Transform Space

Homogeneous Solutions

Homogeneous solutions to the transformed wave equation are found by changing the dependent variable to the product of an amplitude and an elementary wave:

$$F(z) = A(\xi) e^{+ik_z z} \tag{13}$$

$$G(z) = B(\xi) e^{-ik_z z} \tag{14}$$

Equation (13) is intended to satisfy the radiation condition at $z \to \infty$, and Eq. (14) is intended for the radiation at $z \to -\infty$. The new independent variable ξ is selected to map the half-space $0 \le z$ into a finite strip by

$$\xi = -aM_\infty \cos\phi k_r \delta_1 e^{-z/\delta_1} \tag{15}$$

Downwind propagation, where $\cos\phi \ge 0$, is represented by $\xi \le 0$, whereas upwind propagation has $\xi \ge 0$. In either case, the width of the strip is $aM_\infty |\cos\phi| k_r \delta_1$. Crosswind propagation is represented by constant amplitude waves with argument $\xi = 0$.

These changes of variable convert the wave equation to a hypergeometric equation with a single parameter in the denominator of its series solution.[27] The amplitude of the waves traveling upward is

$$A(\xi) = {}_0F_1(1 - 2ik_z\delta_1; \xi) \tag{16}$$

and the wave traveling downward has an amplitude of

$$B(\xi) = {}_0F_1(1 + 2ik_z\delta_1; \xi) \tag{17}$$

The hypergeometric function has a convergent series[27] for finite ξ of

$${}_0F_1(1 + \nu; \xi) = 1 + \sum_{n=1}^{\infty} \frac{\xi^n}{(a + \nu)_n n!} \tag{18}$$

The change of variable [Eq. (15)] maps $z = \infty$ into $\xi = 0$ so that the wave amplitudes $A(\xi)$ and $B(\xi)$ approach unity above the boundary layer. These amplitudes will also be unity for crosswind propagation and will approach unity in the limit of vanishing wind speed. The forms of Eqs. (13) and (14) for the homogeneous solutions are very well suited for understanding the effect of the boundary layer on the acoustic field.

The Wronskian of independent solutions to the wave equation, Eq. (7), is constant because that equation contains no

first derivative term. It may be shown, then, that $F(z)$ and $G(z)$ are independent solutions by evaluating their Wronskian at $z = \infty$ or $\xi = 0$. This evaluation gives

$$W[F(z),G(z)] = F\frac{dG}{dz} - \frac{dF}{dz}G = -2ik_z \tag{19}$$

which confirms that the solutions are independent except at the branch points where $k_z = 0$. The parameter ν in Eq. (18) is a nondimensional value of the Wronskian:

$$\nu = -2ik_z\delta_1 \tag{20}$$

Alternatives to the preceding solutions are the Bessel function solutions used by Chunchuzov.[23] The Bessel functions give an analytic advantage at the expense of the preceding physical interpretation. The two forms are related through an identity, sometimes used to define a Bessel function,[27] which is

$$J_\nu(\zeta) = \frac{(\zeta/2)^\nu}{\Gamma(1+\nu)}\,{}_0F_1(1+\nu;\ -\zeta^2/4) \tag{21}$$

The Bessel function solutions to the present problem are formed by selecting the argument ζ in Eq. (21) to be

$$\zeta = 2\sqrt{aM_\infty \cos\phi k_r\delta_1}\, e^{-z/(2\delta_1)} \tag{22}$$

Changing the sign on the order ν gives an independent solution as long as the order is not an integer. The hypergeometric and Bessel function solutions are related by

$$F(z) = (aM_\infty \cos\phi k_r\delta_1)^{+ik_z\delta_1}\,\Gamma(1+\nu)J_\nu(\zeta) \tag{23}$$

$$G(z) = (aM_\infty \cos\phi k_r\delta_1)^{-ik_z\delta_1}\,\Gamma(1-\nu)J_{-\nu}(\zeta) \tag{24}$$

The complex gamma function has poles at all nonpositive integer arguments, which shows that $F(z)$ has poles at negative integer ν and $G(z)$ has poles at positive integers. These poles originate in the zeroes of the factorial function of Eq. (18). The cuts in the k_r plane restrict k_z to the upper half-plane, and the Wronskian parameter ν is correspondingly restricted to the right half-plane. Thus, we need consider only the poles where $\nu = n > 0$, which occur in the amplitudes B of the incoming waves.

Source Field

Expressions for the field of a monopole source may be developed for either independent pair of homogeneous solutions. The source field expressed in terms of elementary waves with variable amplitude is

$$\hat{\Psi}_s = \frac{\hat{Q}\delta_1}{4\pi^2\nu}\begin{Bmatrix} B(\xi_s)A(\xi), & z > z_s \\ A(\xi_s)B(\xi), & z < z_s \end{Bmatrix} e^{ik_z|z-z_s|} \tag{25}$$

As the wind speed approaches zero, the wave amplitudes approach unity, and the source field expression reduces to its known form without flow. As a function of wave number, the source field expression has poles at the integer values of ν. The Bessel function solutions show these poles clearly. Equations (22) and (23) with the reflection formula for the complex gamma function[27] give

$$\hat{\Psi}_s = \frac{\hat{Q}\delta_1}{4\pi\sin\pi\nu}\begin{Bmatrix} J_{-\nu}(\zeta_s)J_\nu(\zeta), & z > z_s \\ J_\nu(\zeta_s)J_{-\nu}(\zeta), & z < z_s \end{Bmatrix} \tag{26}$$

The point $\nu = 0$ is the previously mentioned branch point in the k_r plane. Poles at the natural integer values of ν lie on the imaginary k_z axis at half-integer intervals. In the k_r plane, these points lie along the hyperbolic segments, where $Re(k_z) = 0$, which originate at the branch points and approach the real axis at $k_r = \pm\infty$. We shall see in the following section that these poles are not present in the expression for the total field, which includes waves reflected from the boundary.

Total Field

The total acoustic field between the source and the ground plane contains waves traveling in both vertical directions. This condition results in a standing wave between the ground and the source. The homogeneous solutions [Eqs. (13) and (14)] will be used to relate this field to the limiting case without flow.

It is not apparent how to use the idea of an image source because of the asymmetry with respect to the ground plane due to the shear flow. Instead, the plane wave reflection coefficient is used to give the total field as a superposition of incident and reflected waves. Either the hypergeometric or the Bessel function solutions may be used to construct the total field. The hypergeometric solutions show the limiting case of no wind, which is Wenzel's solution.[3] The Bessel functions show the extension of Chunchuzov's[23] solution for the effects of source height and ground impedance.

Generalized Hypergeometric Functions

The total field between the ground plane and the source is the sum of the source field and a reflected field that satisfies the radiation condition

$$\hat{\Psi}(z) = \frac{\hat{Q}\delta_1}{4\pi^2\nu}F(z_s)[G(z) + RF(z)], \qquad 0 \le z < z_s \tag{27}$$

where the bracketed term represents incident and reflected plane waves. The reflection coefficient R is determined by the ground boundary condition [Eq. (12)] on $\hat{\Psi}$. The algebra of solving for R is easier if the operator [Eq. (11)] is split into parts to form an expression that is linear in the wind Mach number:

$$L = -\left(\frac{\partial}{\partial z} + i\beta k\right) - M_\infty \cos\phi k_r\left(a\frac{\partial}{\partial\xi} - \frac{1}{k\delta_1}\right) \tag{28}$$

The boundary condition gives the reflection coefficient R,

$$R = -\frac{LG(0)}{LF(0)} \tag{29}$$

or

$$R = \frac{(k_z - \beta k)B_0 + iM_\infty \cos\phi k_r[aB_0' - B_0/(k\delta_1)]}{(k_z + \beta k)A_0 - iM_\infty \cos\phi k_r[aA_0' - A_0/(k\delta_1)]} \tag{30}$$

In the absence of wind or in the crosswind direction, $M_\infty \cos\phi = 0$ and $\xi_0 = 0$, so that the preceding formula for the reflection coefficient reverts to the one without flow. This formula contains the previously mentioned poles in the k_r plane, where ν is a natural integer. These points represent "incident" inhomogeneous waves.

The incident and reflected waves combine to form a standing wave pattern between the ground and the source. The total potential may be expressed as

$$\hat{\Psi}(z) = \frac{\hat{Q}}{4\pi^2}\frac{F(z_s)}{LF(0)}\Theta(z), \qquad 0 \le z < z_s \tag{31}$$

where the function

$$\Theta(z) = \frac{\delta_1}{\nu}[LF(0)G(z) - LG(0)F(z)] \tag{32}$$

represents the standing wave. As $z \to 0$, $\Theta(z) \to 1$ because the bracketed expression in Eq. (32) approaches the Wronskian of $F(z)$ and $G(z)$.

Wenzel's Solution

Equation (31) approaches Wenzel's solution for a source over an impedance plane in the limit of vanishing wind speed.

This limit is found by taking the first terms in the series of Eq. (18) to form first-order asymptotic approximations for the wave amplitudes. Since the standing wave function is unity at the ground surface, the potential $\hat{\Psi}(z)$ is the product $\hat{\Psi}(0)\Theta(z)$. The surface potential is

$$\hat{\Psi}(0) = \frac{\hat{Q}}{4\pi^2}\frac{A(\xi_s)}{LF(0)}e^{ik_z z_s} \tag{33}$$

and

$$LF(0) = -i\left[(k_z+\beta k) + i\frac{M_\infty \cos\phi k_r}{k\delta_1}\right]A_0 - aM_\infty \cos\phi k_r A_0' \tag{34}$$

The wave amplitude and its derivative have asymptotic forms

$$A_0 \sim 1 - \frac{aM_\infty \cos\phi k_r \delta_1}{1+\nu}, \qquad M_\infty \to 0 \tag{35}$$

$$A_0' \sim \frac{1}{1+\nu}, \qquad M_\infty \to 0 \tag{36}$$

The limit of the surface potential for vanishing wind speed is then

$$\hat{\Psi}(0) \sim \frac{i\hat{Q}}{4\pi^2}\frac{e^{ik_z z_s}}{k_z+\beta k}, \qquad M_\infty \to 0 \tag{37}$$

Wenzel's solution[3] is found by using partial fractions to split Eq. (37) into parts representing the hard surface and a radiated wave. The radiated wave is

$$\hat{\Psi}_R(0) = -i\frac{\hat{Q}}{4\pi^2}\frac{\beta k}{k_z(k_z+\beta k)}e^{ik_z z_s} \tag{38}$$

Wenzel's surface wave originates from the pole where $(k_z + \beta k) = 0$, which is the only one possible in the case of no wind. The inverse transform of Eq. (38) may be evaluated by changing the integral over k_x and k_y into an integral over the polar coordinates k_r and ϕ. The integral over ϕ converts the inversion integral into an inverse Hankel transform, so that the radiated wave potential on the surface is

$$\hat{\Psi}_R(0) = -i\beta\frac{\hat{Q}k}{2\pi}\int_0^\infty \frac{k_r J_0(k_r r)}{k_z(k_z+\beta k)}e^{ik_z z_s}\,dk_r \tag{39}$$

The evaluation of this integral was the subject of the papers by Wenzel,[3] Chien and Soroka,[4] Thomasson,[5] and Nobile and Hayek.[6]

Chunchuzov's Solution

Equation (31) reduces to Chunchuzov's solution when the receiver point is on the surface and the admittance is zero. Equation (21) gives Chunchuzov's Bessel function result:

$$\hat{\Psi}(0) = \frac{\hat{Q}}{4\pi^2}\frac{J_\nu(\zeta_s)}{LJ_\nu(\zeta_0)} \tag{40}$$

The boundary condition operator in the preceding expression is modified to use ζ as the independent variable and to evaluate the operation at the boundary where $\zeta = \zeta_0$:

$$L = \frac{\zeta_0}{2\delta_1}\frac{\partial}{\partial\zeta_0} + \frac{M_\infty \cos\phi k_r}{k\delta_1} - i\beta k \tag{41}$$

The standing wave function expressed in terms of Bessel functions is

$$\Theta(z) = \Gamma(1+\nu)\Gamma(1-\nu)\delta_1 L\left[J_\nu(\zeta_0)J_{-\nu}(\zeta) - J_{-\nu}(\zeta_0)J_\nu(\zeta)\right]/\nu \tag{42}$$

Combining the reflection formula and the difference equation[27] for the complex gamma function gives

$$\frac{1}{\Gamma(1+\nu)\Gamma(1-\nu)} = \frac{\sin\pi\nu}{\pi\nu} \tag{43}$$

The Bessel function of negative order is[28]

$$J_{-\nu}(\zeta) = J_\nu(\zeta)\cos\pi\nu - Y_\nu(\zeta)\sin\pi\nu \tag{44}$$

These identities give the standing wave function as

$$\Theta(z) = \pi\delta_1 L p_\nu(\zeta,\zeta_0) \tag{45}$$

where p_ν is the Bessel function cross product[28]

$$p_\nu(\zeta,\zeta_0) = J_\nu(\zeta)Y_\nu(\zeta_0) - J_\nu(\zeta_0)Y_\nu(\zeta) \tag{46}$$

The Bessel function cross-product expression shows that the standing wave function has no poles. The extension of Chunchuzov's results for a receiver above the surface is then

$$\hat{\Psi}(z) = \frac{\hat{Q}}{4\pi^2}\frac{J_\nu(\zeta_s)}{LJ_\nu(\zeta_0)}\Theta(z), \qquad 0 \le z < z_s \tag{47}$$

When the receiver is above the source, ζ and ζ_s are interchanged on the right side of Eq. (47).

Solution in Physical Space

The function for the quasipotential in physical space is given by the Fourier inversion integral of the solution in transform space. If polar coordinates are utilized in both spaces, the inversion integral is

$$\Psi(r,\theta,z,\omega) = e^{-iM_\infty \cos\theta k_r} \times \int_0^\infty\int_0^{2\pi} k_r\, e^{ik_r r\cos(\phi-\theta)}\hat{\Psi}(k_r,\phi,z,\omega)\,d\phi\,dk_r \tag{48}$$

Polar Integral

If the polar integral in Eq. (48) is approximated by the method of steepest descent,[16,23] the integral on ϕ is taken along contours C_1 and C_2 in the complex ϕ plane. Contour C_1 crosses the real ϕ axis at θ at an angle of $-\pi/4$, and contour C_2 crosses at $\theta + \pi$ at an angle of $\pi/4$. A review of the equations leading to $\hat{\Psi}$ shows that

$$\hat{\Psi}(-k_r,\phi+\pi,z,\omega) = \hat{\Psi}(k_r,\phi,z,\omega) \tag{49}$$

which allows the inversion integral [Eq. (48)] to be approximated by the two-sided inversion integral on k_r:

$$\Psi(r,\theta,z,\omega) \approx e^{-i(M_\infty \cos\theta k_r + \pi/4)} \times \int_{-\infty}^{+\infty} k_r\sqrt{2\pi/k_r r}\, e^{ik_r r}\hat{\Psi}(k_r,\theta,z,\omega)\,dk_r \tag{50}$$

Radial Integral

The radial wave-number integral in Eq. (50) is evaluated with a closed contour in the upper half of the k_r plane. The integral along the real axis is equal to the sum of the integrals around the poles of $\hat{\Psi}(k_r,\theta,z,\omega)$ plus an integral along the branch cut. The branch integral is called the lateral wave[16,23] and corresponds to a direct ray from the source to the receiver.[16] It has a spherical spreading characteristic, varying with distance as $1/r$. The residue contributions vary with distance as $1/\sqrt{r}$, so that the residue terms dominate at large distance. Here, we are interested in the case of long-range downwind propagation so that the lateral wave can be omitted.

The total potential is the sum of the potentials of the normal modes. Each mode is given by an integral around a pole of $\hat{\Psi}$. Equation (31) for the potential transform gives

$$\Psi_n(r,\theta,z,\omega) = \frac{\hat{Q}}{4\pi^2} e^{-i(M_\infty \cos\theta k_r + \pi/4)} \times \oint k_r\sqrt{2\pi/k_r r}\, e^{ik_r r} \frac{F(z_s)}{LF(0)} \Theta(z)\, dk_r, \qquad 0 \le z < z_s \quad (51)$$

The poles in the k_r plane depend on the propagation direction θ. In the downwind direction, these poles are found near imaginary values of k_z so that the Wronskian ν is nearly a real number. The number of poles increases with increasing source frequency and with boundary-layer thickness. The number of poles also increases with wind speed. For low frequencies and wind speed, there is a single pole. If the ground were absorbing, then the Wronskian ν would correspond to Wenzel's surface wave pole in the limit of no wind.

In the study of downwind propagation over fairly hard ground where β is small, it is convenient to use ν as the independent variable in numerical solutions for the poles. The differential of the dispersion equation gives

$$\frac{d\nu}{dk_r} = 4\frac{k_r}{\nu}\delta_1^2 \quad (52)$$

and the standing wave function has a simplified form at the poles, since $LF(0) = 0$:

$$\Theta(\nu_n;z) = -\frac{\delta_1}{\nu_n} LG(\nu_n;0)F(\nu_n;z) \quad (53)$$

The residue theorem, assuming simple poles, thus gives the potential for each mode n as

$$\Psi_n(r,\theta,z) = C_n\sqrt{2\pi/(R_{rn}r)}\, e^{i(k_{rn} - M_\infty \cos\theta k)r}\Theta(\nu_n;z_s)\Theta(\nu_n;z) \quad (54)$$

where

$$C_n = \frac{\hat{Q}}{2\pi\delta_1} e^{-3\pi i/4}\left[4\delta_1^2 LG(\nu_n;0)\frac{\partial LF(\nu_n;0)}{\partial\nu}\right]^{-1} \quad (55)$$

Since the traveling wave and standing wave expressions are proportional in a normal mode, Eq. (54) is valid for receiver positions above and below the source.

Figure 2 shows three normal modes Θ_n computed for the application to wind turbine noise described in the next section. The lowest mode decays monotonically to approach zero at about two boundary-layer thicknesses. The central mode has a single-phase reversal and becomes perceptually zero at about five thicknesses; the highest mode has two phase reversals before beginning a monotone decay. This example suggests that the higher modes will have their greatest influence outside the boundary layer, whereas the lowest mode is felt primarily within the boundary layer.

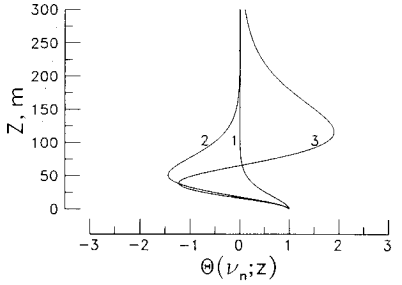

Fig. 2 Downwind acoustic modes for an atmospheric boundary layer over a hard surface.

Low-Wind Approximation

A single mode can be approximated by the asymptotic equation, Eq. (34), for $LF(0)$ in the case of low wind speed. Since $A'(k_z;0)$ is of the order of M_∞, there will be a solution of Eq. (34) which approaches $k_z = -k\beta$ as M_∞ approaches zero. This is the singularity that leads to the surface wave studied by Wenzel. The asymptotic equations, Eqs. (35) and (36), substituted into Eq. (34) give an approximation for the a single-mode wave number. Since the Wronskian ν is proportional to k_z, it is eliminated to give

$$k_{z1} \sim \left[-\beta + 2i\sqrt{1-\beta^2}\left(\frac{k\delta_1 - i\beta}{1 + 2ik\delta_1\beta}\right)M_\infty \cos\theta\right]k \qquad M_\infty \to 0 \quad (56)$$

$$k_{r1} \sim \left[\sqrt{1-\beta^2} + 2i\beta\left(\frac{k\delta_1 - i\beta}{1 + 2ik\delta_1\beta}\right)M_\infty \cos\theta\right]k \qquad M_\infty \to 0 \quad (57)$$

These formulas are valid to the first order in M_∞. The ground admittance β does not have to be small but must have magnitude less than unity, $|\beta| < 1$. If the ground is hard so that β is small, then

$$k_{r1} \sim [1 + 2ik\delta_1\beta M_\infty \cos\theta]k, \qquad M_\infty \to 0, \quad |\beta| \ll 1 \quad (58)$$

The attenuation rate of the propagating mode is the imaginary part of k_{r1}:

$$\alpha_{r1} \sim 2k^2\delta_1 Re(\beta) M_\infty \cos\theta \quad (59)$$

This attenuation rate is proportional to the frequency squared, the boundary-layer thickness, the real part of the ground admittance, and the component of wind speed in the direction of the observer.

Small-Admittance Approximations

Chunchuzov has shown that the roots k_{rn} are clustered near the plane wave number k when $k\delta_1$ is large, that is, when the boundary-layer thickness is large compared to a wavelength. The function $LJ_\nu(\zeta_0)$ is found to be more sensitive to variations in the order ν than to the argument ζ_0. Chunchuzov takes advantage of this condition to approximate the roots by the first term of the McMahon expansion[28] for the zeroes of $J_\nu'(\zeta_0)$. This approximation shows the clustering quality of the modes, but its accuracy decreases with frequency and is inadequate for the application to wind turbine noise considered here.

An approximation for the effect of small admittance on the modes is found by taking the total differential of $LF(\nu_n;0)$ with β as an independent variable:

$$dLF(\nu_n;0) = \frac{\partial LF(\nu_n;0)}{\partial\beta} d\beta + \frac{\partial LF(\nu_n;0)}{\partial\nu} d\nu = 0 \quad (60)$$

The second coefficient in Eq. (60) is the same term as in Eq. (55) because β is constant in the physical problem. The first coefficient is readily available because $LF(\nu_n;0)$ is linear in β. The derivative of the characteristic value ν_n with respect to the admittance is then

$$\frac{d\nu_n}{d\beta} = ikA_0(\nu_n)\left[\frac{\partial LF(\nu_n;0)}{\partial\nu}\right]^{-1} \quad (61)$$

The preceding derivative, evaluated for a hard surface where $\beta = 0$, gives a two-term Taylor series for the radial wave number of each mode:

$$k_{rn} = k\left\{\sqrt{1 + \nu_n^2/4k^2\delta_1^2} + i\nu_n A_0(\nu_n)\left[\delta_1\frac{\partial LF(\nu_n;0)}{\partial\nu}\right]^{-1}\beta\right\} \quad (62)$$

The characteristic values ν_n, if any, are real when $\beta = 0$. We number these values in order of decreasing magnitude, $\nu_1 > \nu_2 > \nu_3 \ldots$, so that the first mode decays most rapidly with height. Consequently, the phase speed ω/k_{r1} of the first mode will be the least, and the speed of the last mode will be greatest. The attenuation rate of the mode is proportional to the real part of the admittance, as shown in Eq. (62). Although it is not obvious that this proportionality factor, the bracketed term in Eq. (62), must be positive, we have observed it to be so in all computations made for downwind propagation.

Medicine Bow Wind Turbine

Ground Impedance

Ground impedance was measured on-site using the Zuckerwar[12] meter. These data, presented as admittance, are shown in Fig. 3 with the Delany-Bazley[7] and the Attenborough[13] models. At low frequencies, the ρc term in the Delany-Bazley formula is negligible in comparison to the frequency-dependent terms. These latter terms give an admittance approximation

$$\beta \approx 10.4(\rho_0 f/\sigma)^{0.75} e^{-1.0i} \tag{63}$$

A ground flow resistance $\sigma = 1.82 \times 10^5$ N · s/m^4 with standard atmospheric density ρ_0 gives the best fit to our measured admittance data. The low-frequency Attenborough formula is

$$\beta \approx 2.23(\rho_0 f/\sigma)^{0.50} e^{-0.79i} \tag{64}$$

A larger flow resistance, $\sigma = 4.71 \times 10^5$ N · s/m^4, is needed to fit the Attenborough formula to the measured admittance. A line fit to the data, assuming constant phase and a typical value $\sigma = 2.5 \times 10^5$ N · s/m^4, gives

$$\beta \approx 23.3(\rho_0 f/\sigma)^{0.82} e^{-1.38i} \tag{65}$$

Figure 3 shows that the models represent bounds to the magnitude of the admittance in our limited range of frequencies. The Attenborough model has the largest magnitude and smallest phase and is expected to predict, based on Eq. (59), the largest attenuation. Similarly, the site data admittance should give the smallest attenuation because of its large phase. The phase of the measured admittance is surprisingly large. The Medicine Bow tests were made during a rainy part of the season when the ground was saturated in many places. Zuckerwar[12] has noted that moisture causes the phase of the admittance to increase, so that these conditions may account for the phase differences between the measured admittance and the models, which are more appropriate for nearly dry media.

Wind Profile

Wind speeds were measured by a tethered balloon instrument package. Wind speed profiles are shown in the Fig. 4 for day and night conditions. Wind profiles varied with time of day and weather conditions (cloudy or clear), so that data from several profiles were grouped to represent typical conditions. The day profile is representative of midday on a clear day. The night profile is representative of 2 h after sunset on a clear night. Profiles were quantified by fitting exponential curves to the measured wind data. Daytime data show a thin boundary layer, on the order of 1 or 2 m. An exponential profile using $\delta_1 = 1.2$ m and $U_\infty = 9.8$ m/s gives the best fit to the daytime data; however, the exponential does not follow the data very well. Although the ground boundary layer is thin, the winds above the ground follow a sort of "S"-shaped curve between 25 and 250 m in height. Nighttime data show a thick boundary layer extending above the hub of the wind turbine. The exponential fit to these data has $\delta_1 = 50.6$ m and a higher wind speed limit, $U_\infty = 12.8$ m/s. These data are a much better match to the assumed exponential profile than the daytime data.

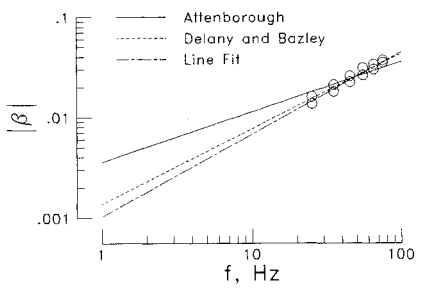

Fig. 3 Ground admittance at the Medicine Bow wind turbine.

Noise Propagation Data

The wind turbine acoustic data were measured with ground-level microphones. The downwind data were measured with a nine-microphone array extending 0.35–20 km from the wind turbine. The acoustic data were recorded in the field and later reduced with Fourier analysis. The acoustic data presented here are average values of the sound pressure levels at harmonics of the blade-passage frequency of 1 Hz. Results will be given for day and night averages. Each average group was formed from data runs that were measured under conditions characterized as similar to the day and night wind profiles illustrated in Fig. 4. A 3-dB signal-to-noise ratio was required for a particular harmonic level estimate to be included in the sample. The average day results are based on five runs that together encompass 18 min of data. The average night results are based on seven runs that encompass 25 min of data. The data exhibit a large amount of variability. The measurements were made in wind conditions that, under normal outdoor acoustic measurement standards, would have been deemed unacceptable. Variations of wind speed, profile, direction, and turbulence had a major impact on the wind turbine as an acoustic source and on the subsequent propagation of the wind turbine noise.

Theory/Measurement Comparison

Normal mode predictions are compared to the average data for day and night conditions in Figs. 5 and 6, respectively. The average data are shown as solid symbols, with the standard deviations indicated by the length of the superimposed "I" symbols. The decay of the data with distance is roughly the

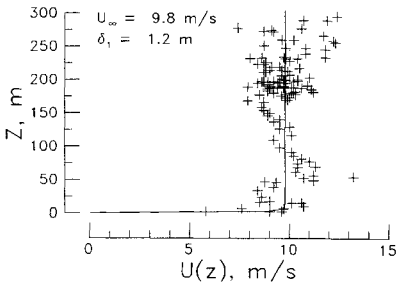

a) Typical daytime conditions

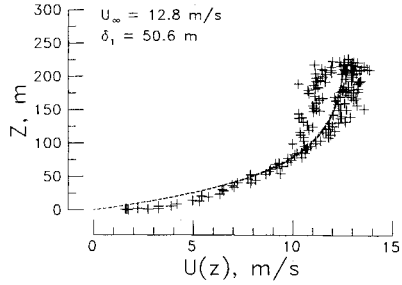

b) Typical nighttime conditions

Fig. 4 Wind speed profiles at the Medicine Bow wind turbine.

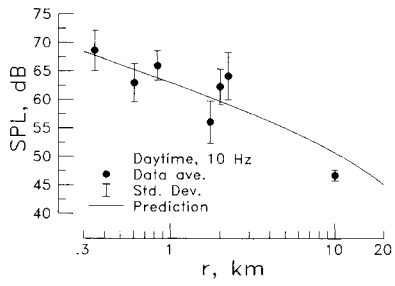

Fig. 5 Daytime downwind noise propagation at Medicine Bow (10 Hz, one normal mode).

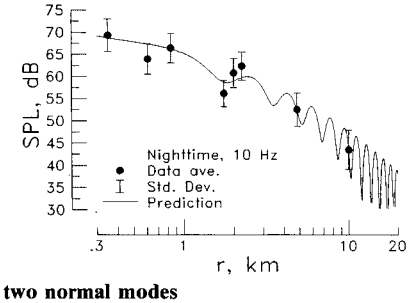

a) 10 Hz, two normal modes

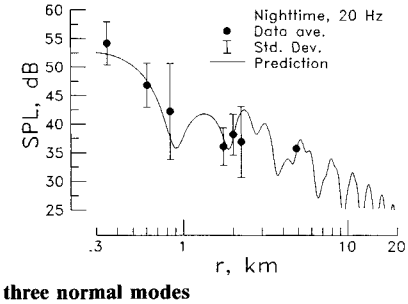

b) 20 Hz, three normal modes

Fig. 6 Nighttime downwind noise propagation at Medicine Bow.

$1/\sqrt{r}$ law of the preceding theory. This observation is true for the frequency range 5–20 Hz. At large distances, the data deviate from the $1/\sqrt{r}$ trend. This deviation is an additional attenuation that is predicted to be much greater than that due to atmospheric absorption. Results are given for 10 Hz in Fig. 5 and for 10 and 20 Hz in Fig. 6. The predicted curves are best fits to the data. That is, the predicted curves are based on acoustic source strengths chosen such that the mean error between the predicted curve and the data is zero. A rms error is then calculated between the predicted curve and the data. The Attenborough impedance model, illustrated in Fig. 3, was used in the predictions. A source height of 50 m was used for both day and night predictions. This height represents an effective source three-quarters of the distance from the hub to the tip of a downward pointing blade. For the daytime wind profile, the wind turbine acoustic source location is well above the idealized boundary layer. The predictions for the daytime wind profile were not sensitive to source location, because only a single mode is propagating. The wind turbine source location is within the boundary layer for the nighttime wind profile, and the predictions were sensitive to source position because, at the higher frequencies, several modes were propagating. Night predictions were made with source heights of 40, 50, and 60 m. An analysis of the rms error between the predictions and the data for these three source heights did not indicate one source height as having a better overall agreement with the data than the others. A source height of 50 m was used for the night prediction, based on the typical 75% span source location used in propeller noise theory.

The agreement between the normal mode theory and the data is judged overall as fair to good. The agreement is better for the night wind profile results. The monotonic decay of

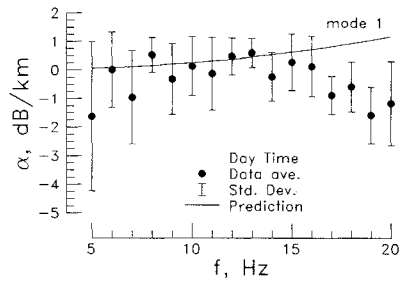

a) Daytime conditions, one normal mode

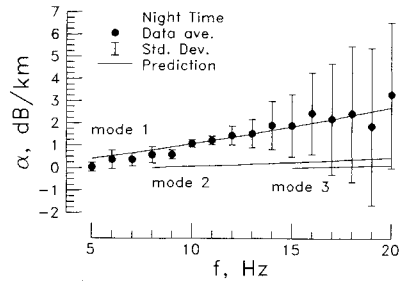

b) Nighttime conditions, three normal modes shown separately

Fig. 7 Downwind noise attenuation at Medicine Bow.

predicted levels vs range for the day is because only a single mode is propagating. For the higher frequencies, multiple propagating modes are predicted at night. Two modes are propagating between 8 and 15 Hz and three modes above 15 Hz. These modes travel at slightly different speeds, so that they may reinforce or cancel at different distances. The interaction of these multiple modes causes the interference, the local maxima and minima, observed in the predictions. The data also suggest an interference pattern, although a smaller microphone spacing would be needed to show this clearly.

Predicted and Measured Attenuation Coefficients

Normal mode theory predicts a propagation attenuation in addition to the $1/\sqrt{r}$ divergence. To obtain a measurement of this attenuation, the acoustic data from each run were corrected for cylindrical spreading. The slope of a least-squares-fit line through the corrected data is proportional to the experimental attenuation coefficient. If there is only a single propagating mode, the experimental attenuation may be compared directly to the theoretical attenuation, which is predicted to be a straight line in terms of SPL vs distance. When there are several propagating modes, the theoretical curve is the log of the sum of several exponentials and hence not a straight line. Although several modes are predicted at higher frequencies and larger boundary-layer thicknesses, we still use a straight line through the data as an effective measure of attenuation. The average and standard deviations of the attenuation coefficients were calculated from the results of the individual runs comprising the day and night data groups. These attenuation coefficient statistics are compared to attenuation predictions for the day and night wind profiles in Fig. 7. The Attenborough impedance model was used in the predictions. Use of any one of the three impedance models illustrated in Fig. 3 had little effect on the predicted day attenuations. The impedance model chosen had a greater effect on the predicted night attenuations. The Attenborough model, as stated earlier, gives the largest predicted attenuation. The Attenborough model was chosen for the normal mode predictions presented in this paper based on the good agreement between the night profile predicted and measured attenuation coefficients using the model.

The agreement between the measured and predicted attenuation coefficients is fair, at best, for the day. The scatter in the day SPL measurements obscured the calculated attenuation coefficient results. The nighttime measured attenuation is in good agreement with the first-mode predictions, even for fre-

quencies greater than 7 Hz, where multiple modes are predicted. At these frequencies, because of the multiple modes, the procedure for calculating the measured coefficients from the data is less valid for a direct comparison with the predicted coefficients. The fact that the measured results continue to agree with the predicted first-mode attenuation coefficients at high frequency implies that the strength of the first mode is greater than the higher modes. The reader is reminded here of the mode-numbering convention described earlier, which must be kept in mind while interpreting these results.

Conclusions

The normal mode theory of Chunchuzov has been extended to include the effect of finite ground plane impedance and the effect of source height. The impedance extension is made via a simple modification to Chunchuzov's boundary condition operator. The source height extension is made by introducing a standing wave function. This function multiplies the Chunchuzov solution when both functions are expressed as Fourier transforms. The standing wave function is an entire function of the radial wave number so that the generalized solution does not require additional branch cuts or introduce new poles in the evaluation of the inverse transform.

The transform solution for a point source in an exponential-profile boundary layer is given by a sum of nonhomogeneous waves, plane waves with "nearly imaginary" vertical components of wave number, with variable amplitudes. The amplitude functions are given by the generalized hypergeometric function ${}_0F_1$.

The normal mode solution is, in the limit of vanishing wind speed, asymtotic to the surface wave solution studied by Wenzel. The pole yielding the first normal mode is the singularity that gives the surface wave when the wind speed is zero. In this sense, the Chunchuzov normal mode spectrum is a surface wave spectrum.

The normal mode theory has been applied to predict long-range downwind propagation of low-frequency wind turbine noise. Data from a wind turbine at Medicine Bow, Wyoming, were measured under typical daytime conditions, where the atmospheric boundary layer was thin, and under nighttime conditions, where the boundary layer was thick. Acoustic measurements were made with nine ground-level microphones placed 0.35–20 km downwind of the turbine. Frequency analysis of the data defined harmonics of the blade-passage frequency of 5–20 Hz. The levels of these harmonics had large variability, with standard deviations of 5–8 dB from the averages, depending on the frequency, downrange distance, and wind condition. The daytime wind data also had large variability, but the nighttime data had less variability and followed an exponential profile up to about 200 m. Noise predictions based on typical daytime wind conditions showed a fair agreement with the measured data. In particular, both theory and experiment indicate a cylindrical spreading characteristic and an additional attenuation that depends on frequency and distance. Predictions for typical nighttime winds showed better agreement than in the day, presumably due to the more stable wind profiles. The normal mode theory predicted that the long-range acoustic field would be composed of contributions of up to three modes in the nighttime boundary layer and at the higher frequencies. Interactions of these modes, which propagate at slightly different speeds, caused a complex interference pattern in the predictions. The nighttime acoustic data also suggested an interference phenomenon, but there were not enough microphones to define this interference clearly. Thus, although the normal mode theory appears to offer a plausible model for the effect of winds on low-frequency sound propagation, a more detailed experimental verification is needed to draw firm conclusions.

References

[1]Blokhintsev, D. I., "Acoustics of a Nonhomogeneous Moving Medium," NACA TM-1399, 1946.

[2]Pierce, A. D., *ACOUSTICS: An Introduction to Its Physical Principles and Applications,* McGraw-Hill, New York, 1981.

[3]Wenzel, A. R., "Propagation of Waves Along an Impedance Boundary," *Journal of the Acoustical Society of America,* Vol. 55, May 1974, pp. 956–963.

[4]Chien, C. F. and Soroka, W. W., "Sound Propagation Along an Impedance Plane," *Journal of Sound and Vibration,* Vol. 43, No. 1, Nov. 1975, pp. 9–20.

[5]Thomasson, S.-I., "Reflection of Waves from a Point Source by an Impedance Boundary," *Journal of the Acoustical Society of America,* Vol. 59, April 1976, pp. 780–785.

[6]Nobile, M. A. and Hayek, S. I., "Acoustic Propagation Over an Impedance Plane," *Journal of the Acoustical Society of America,* Vol. 78, Oct. 1985, pp. 1325–1336.

[7]Delany, M. E. and Bazley, E. N., "Acoustical Properties of Fibrous Absorbent Materials," *Applied Acoustics,* Vol. 3, No. 2, April 1970, pp. 105–116.

[8]Chessell, C. I., "Propagation of Noise Along a Finite Impedance Boundary," *Journal of the Acoustical Society of America,* Vol. 62, Oct. 1977, pp. 825–834.

[9]Parkin, P. H. and Scholes, W. E., "The Horizontal Propagation of Sound from a Jet Engine Close to the Ground, at Radlett," *Journal of Sound and Vibration,* Vol. 1, Jan. 1964, pp. 1–13.

[10]Parkin, P. H. and Scholes, W. E., "The Horizontal Propagation of Sound from a Jet Engine Close to the Ground, at Hatfield," *Journal of Sound and Vibration,* Vol. 2, No. 4, Oct. 1965, pp. 353–374.

[11]Embleton, T. W. F., Piercy, J. E., and Olson, N., "Outdoor Sound Propagation Over Ground of Finite Impedance," *Journal of the Acoustical Society of America,* Vol. 59, Feb. 1976, pp. 267–277.

[12]Zuckerwar, A. J., "Acoustic Ground Impedance Meter," *Journal of the Acoustical Society of America,* Vol. 73, June 1983, pp. 2180–2186.

[13]Attenborough, K., "Acoustical Characteristics of Rigid Fibrous Absorbents and Granular Materials," *Journal of the Acoustical Society of America,* Vol. 73, March 1983, pp. 785–799.

[14]Attenborough, K., Hayek, S. I., and Lawther, J. M., "Propagation of Sound Above a Porous Half-Space," *Journal of the Acoustical Society of America,* Vol. 68, Nov. 1980, pp. 1493–1501.

[15]Pekeris, C. L., "Theory of Propagation of Sound in a Half-Space of Variable Sound Velocity Under Conditions of Formation of a Shadow Zone," *Journal of the Acoustical Society of America,* Vol. 18, Oct. 1946, pp. 295–315.

[16]Brekhovskikh, L. M., *Waves in Layered Media,* 2nd ed., Academic, New York, 1980.

[17]Van Moorhem, W. K. and Landheim, G. K., "The Propagation of Plane Waves in a Thermally Stratified Atmosphere," *Journal of the Acoustical Society of America,* Vol. 76, Sept. 1984, pp. 867–870.

[18]Raspet, R., Lee, S. W., Kuester, E., Chang, D. C., Richards, W. F., Gilbert, R., and Bong, N., "A Fast-Field Program for Sound Propagation in a Layered Atmosphere Above an Impedance Ground," *Journal of the Acoustical Society of America,* Vol. 77, Feb. 1985, pp. 345–352.

[19]Grossard, E. E. and Hooke, W. H., *Waves in the Atmosphere,* Elsevier, Amsterdam, 1975.

[20]Pridmore-Brown, D. C., "Sound Propagation in a Temperature- and Wind-Stratified Medium," *Journal of the Acoustical Society of America,* Vol. 34, April 1962, pp. 438–443.

[21]Rasmussen, K. B., "Outdoor Sound Propagation Under the Influence of Wind and Temperature Gradients," *Journal of Sound and Vibration,* Vol. 104, No. 2, Jan. 1986, pp. 321–335.

[22]Koutsoyannis, S. P., "Characteristics of Acoustic Disturbances in Linearly Sheared Flows," *Journal of Sound and Vibration*, Vol. 68, No. 2, Jan. 1980, pp. 187–202.

[23]Chunchuzov, I. P., "Field of a Low-Frequency Point Source of Sound in an Atmosphere with a Nonuniform Wind-Height Distribution," *Soviet Physics—Acoustics,* Vol. 30, July-Aug. 1984, pp. 323–327.

[24]Willshire, W. L., Jr., "Long Range Downwind Propagation of Low-Frequency Sound," NASA TM 86409, April 1985.

[25]Zorumski, W. E. and Willshire, W. L., Jr., "The Acoustic Field of a Point Source in a Uniform Boundary Layer Over an Impedance Plane," AIAA Paper 86-1923, July 1986.

[26]Willshire, W. L., Jr. and Zorumski, W. E., "Low-Frequency Acoustic Propagation in High Winds," *NOISE-CON 87 Proceedings: High Technology for Noise Control,* Institute of Noise Control Engineering, 1987, pp. 275–280.

[27]Rainville, E. D., *Special Functions,* Macmillan, New York, 1960.

[28]Olver, F. W. J., "Bessel Functions of Integer Order," *Handbook of Mathematical Functions with Formulas, Graphs, and Mathematical Tables,* National Bureau of Standards, Washington, DC, June 1964, pp. 355–434.